2018 IEEE/RSJ International Conference on Intelligent Robots and Systems (IROS)
Madrid, Spain, October 1-5, 2018

A Soft Robot to Navigate the Lumens of the Body Using Undulatory Locomotion Generated by a Rotating Magnetic Dipole Field

Lan N. Pham and Jake J. Abbott

***Abstract*— In this paper, we describe a soft-robotic actuation concept to enable a mesoscale medical robot to navigate the natural lumens of the body, such as blood vessels and intestines. The concept comprises a simple soft robot with two embedded permanent magnets with alternating magnetic polarity, and a rotating (nonuniform) dipole magnetic field that is swept over the robot, resulting in a traveling-wave undulatory motion that propels the robot forward and backward. This soft-actuation technology can be fabricated in a wide range of sizes due to its simplicity, and has the potential to be applied in a variety of diagnostic and therapeutic contexts. We conduct experiments and numerical simulations to verify the movement of the soft robot. Then, we confirm the benefits of using nonuniform dipole fields over using uniform fields, as well as the benefits of alternating the polarity of the magnets embedded in the device.**

I. Introduction

In this paper, we describe a soft-robotics actuation concept to enable a mesoscale medical robot to navigate the natural lumens of the body, such as blood vessels and intestines. The method comprises a simple "robot" that is a soft structure with two embedded permanent magnets (e.g., at the two ends of the structure) with *alternating magnetic polarity*, and a rotating *nonuniform* magnetic field that is swept over the robot, resulting in an undulatory motion (i.e., traveling wave) that propels the robot forward (Fig. 1). When the rotation of the magnetic field is reversed, the direction of the robot is also reversed. Since this actuation concept is wireless, and because it has no internal moving parts beyond mechanical compliance, this soft-actuator concept is capable of being fabricated at a wide range of scales. In addition, because a permanent magnet can be fabricated as an annulus, the robot can be fabricated with an internal lumen without interfering with the actuation.

For the applied rotating nonuniform magnetic field, we will exclusively consider magnetic *dipole* fields. A dipole field has a simple analytic structure that facilitates analysis. Dipole fields are generated by spherical permanent magnets, but the fields of all magnetic sources can be approximated by dipole fields at sufficient distances. Certain permanent-magnet geometries can be accurately approximated as dipole fields at even relatively close distances [1]. Our group has developed spherical-permanent-magnets [2] and electromagnetic [3] sources whose fields are accurately approximated by dipole fields, and we have developed methods to generate rotating magnetic fields at arbitrary locations in space and about arbitrary axes using those dipole-field sources [4]. In this paper, we compare the use of dipole fields to uniform magnetic fields. We do not explicitly consider any other nonuniform magnetic fields; however, the results are likely to apply to any field source that is sufficiently dipole-like.

The authors are with the Department of Mechanical Engineering and the Robotics Center, University of Utah, USA. lan.pham@utah.edu, jake.abbott@utah.edu

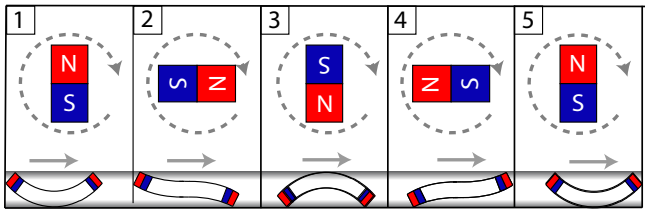

Fig. 1: Concept image (not shown to scale) of the soft robot's undulatory locomotion (from left to right) through a lumen as it interacts with the rotating dipole field.

A number of groups have developed bioinspired actuation technologies to enable robotic locomotion through lumens, some utilizing applied magnetic fields. Kim et al. [5] and Nam et al. [6] have developed magnetic-actuation concepts that utilize a uniform rotating field and a uniform oscillating field, respectively, to generate snake-like propulsion. Both concepts comprise a series of articulated magnetic segments with protruding legs to cause asymmetric friction with lumen walls when driven by the applied magnetic field. In both of the prototypes developed, the entire device is dedicated to accomplishing the novel locomotion scheme, and it is not clear how the concepts could be incorporated into a more traditional medical device. Due to the complexity of the respective designs, neither are inherently scalable.

Diller et al. [7] and Hu et al. [8] created a concept similar in function to that of [5], but with a simpler mechanical design: a flat sheet of magnetic material is rolled up before magnetization, without requiring articulated segments. They demonstrated multiple gaits with a millimeter-scale prototype using uniform rotating magnetic fields.

Another related concept from Kim et al. [9] resulted in a miniature robot that crawls across a surface using a looping inchworm gait (i.e., reminiscent of an "inchworm" moth larva). This type of motion involves two feet, each taking turns anchoring to the ground as its body contracts and propels itself forward. Their concept again uses a uniform rotating magnetic field for actuation, with the miniature device comprising two magnetic bodies separated by a compliant structure. The device also comprises a number of additional mechanical elements that are required to transduce the magnetic field into locomotion and stop the permanent-magnet elements from sticking together. A related nonmagnetic device capable of inchworm locomotion was developed that

utilizes shape-memory-alloy fibers embedded longitudinally within a soft body for actuation [10].

Other methods to locomote through tubes have been inspired by earthworm locomotion, utilizing rectilinear (i.e., straight line) motion. This type of actuation works by segments in the device sequentially widening and narrowing to change the friction properties of the respective segments with respect to the lumen walls [11]–[14]. A similar rectilinear motion can be created even when the segments are not able to individually widen and narrow, simply by capitalizing on the friction imbalance when only one segment is moving relative to multiple stationary segments [15]. In these rectilinear locomotion concepts, all of the motion is generated internally or come from a tether, unlike methods that utilize applied magnetic fields. As a result, the actuators within the robot have increased complexity relative to the magnetic concepts, making them more challenging to scale down to the size that would be desirable for many medical applications.

Our actuation concept has similarities with the magnetic-actuation concepts described above. The fundamental difference is that we utilize a rotating nonuniform field (specifically, a rotating dipole field), as opposed to a rotating uniform field (e.g., generated by tri-axial Helmholtz coils). In a uniform field, all magnetic elements experience the same field as each other at all times, so in a sense, the "nonuniformity" must be introduced in the mechanical design of the device to break the symmetry and cause locomotion in some specific direction. Our use of a nonuniform field enables the design of the soft robot to be substantially simpler, and as a result enables fabrication at smaller scales. In addition, translating bench-top results that utilize tri-axial Helmholtz coils to a clinical system will be substantially more challenging than translating concepts that utilize nonuniform fields, because it is easier to place a strong magnetic dipole source near and adjacent to a patient than it is to fully surround that patient with coils.

This soft actuation concept was developed particularly for medical applications, across scales. The technology can be applied in untethered devices ranging from microrobots, for which there are numerous potential medical applications throughout the human body [16], [17], to capsule endoscopes for screening, diagnosis, and therapy in the gastrointestinal (GI) tract [18], [19]. It may also be possible to place our proposed soft actuator at the distal end of continuum devices such as catheters and endoscopes, while still allowing fluid flow. This would enable the tip of the device to assist in propulsion by moving itself forward as the device is pushed from the proximal end. It might even be possible to expand this concept to have alternating-polarity magnets distributed along the entire length of the continuum device.

In this paper, we first perform an experimental study comparing rotating *dipole* and *uniform* applied magnetic fields, and *alternating* and *nonalternating* embedded-magnet polarities (Fig. 2), and we find that our proposed combination results in the best propulsion. Afterward, we perform a simple numerical study to provide some additional insight into the experimental results.

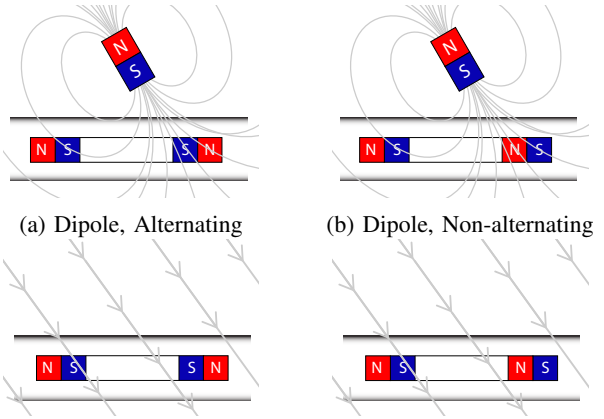

(a) Dipole, Alternating (b) Dipole, Non-alternating

(c) Uniform, Alternating (d) Uniform, Non-alternating

Fig. 2: The four cases considered in the experimental study.

II. Why Rotating Dipole Fields and Embedded Magnets with Alternating Polarity?

Our concept used two permanent magnets with alternating polarity embedded in the soft robot and rotating nonuniform (dipole-like) field that sweeps over the robot to induce a traveling wave. Each of the permanent magnets has a magnetic dipole $\boldsymbol{m}$ that points along the axis of the magnets. When a magnetic dipole $\boldsymbol{m}$ is placed in a magnetic field $\boldsymbol{b}$, a torque $\boldsymbol{\tau}$ is induced, which attempts to align the dipole with the applied field:

$$\boldsymbol{\tau} = \boldsymbol{m} \times \boldsymbol{b} \tag{1}$$

and a force $\boldsymbol{f}$ is induced due to the spatial derivative in the applied field, which attempts to translate the dipole to a location with a stronger field:

$$\boldsymbol{f} = (\boldsymbol{m} \cdot \nabla)\boldsymbol{b} \tag{2}$$

The dipole field generated by some actuator dipole $\boldsymbol{m}_a$ at each point $\boldsymbol{p}$ in space:

$$\boldsymbol{b}(\boldsymbol{p}) = \frac{\mu_0}{4\pi\|\boldsymbol{p}\|^5}\left(3\boldsymbol{p}\boldsymbol{p}^T - \mathcal{I}\|\boldsymbol{p}\|^2\right)\boldsymbol{m}_a \tag{3}$$

decays as $\sim \|\boldsymbol{p}\|^{-3}$ (as does the torque that it generates on some other dipole), and the spatial derivatives decay as $\sim \|\boldsymbol{p}\|^{-4}$ (as does the force that it generates on some other dipole). As a result, when projecting magnetic fields over distances, the effects of magnetic torque tend to dominate those of magnetic force. In a uniform field (e.g., generated by tri-axial Helmholtz coils), there are negligible differences spatially in the field, and as a result their are negligible forces on the embedded magnets.

A simple way to think about the hypothesized beneficial effect of using a rotating nonuniform (dipole) field is that the magnets embedded in the soft robot experience approximately the same field as each other, but out of phase (e.g., one magnet experiences a component of the rotating field before the other, as depicted in frames 2 and 4 of Fig. 1), because the magnets are located at distinct, albeit close, points in the field. The result is that a rotating field will cause a traveling wave in a certain deterministic direction; if the

field rotation is reversed, then the direction of the traveling wave will also reverse. As the wave travels across the robot's body, any portion of the robot in contact with the lumen will move less than portions not in contact (due to friction with the lumen's walls), resulting in an undulatory locomotion in a deterministic direction. In contrast, in a uniform field we expect the field to bend the robot, but with nothing to cause a net translation in some specific direction (at least not due to torque-based bending).

The polarization of the permanent magnets embedded in the soft robot is also hypothesized to be important. In the case of alternating magnets, which we propose, the magnetic torques applied to the two magnets will tend to be opposite one another, which will excite the first bending mode (i.e., result in a single large-amplitude arc, as depicted in frames 1, 3, and 5 of Fig. 1). With non-alternating magnets, the magnetic torques applied to the two magnets will tend to be approximately the same as one another, which will excite the second bending mode (i.e., result in a sinusoidal shape with two small-amplitude arcs). It is our conjecture that larger deflections will cause larger contractions per half cycle (particularly as the field strength decreases), and will enable greater distances to be traversed in a single cycle.

III. Experimental Study of Robot Propulsion

A. Apparatus

1) Omnimagnet: An Omnimagnet (Fig. 3a) is a device with a cubic form-factor comprising three densely packed, mutually orthogonal electromagnetic coils surrounding a spherical ferromagnetic core [3]. The Omnimagnet is capable of generating dipole-like fields by controlling the three currents sourced to its coils. The dipole moment of an Omnimagnet is composed of two parts—the dipole moment of the electromagnetic coils, and the dipole moment of the ferromagnetic core that is magnetized by the coils—and both parts are approximately linear with respect to the applied currents (for the magnitude of currents considered here). The Omnimagnet was optimized to be accurately modeled by the point-dipole model (3), and that model is quite accurate at distances (from its center) greater than 1.5 minimum-bounding-sphere radii. The Omnimagnet used in our experiments here is of the type described in [20]; it has a cubic dimension of 127 mm, a minimum-bounding-sphere radius of 90 mm, and a maximum dipole strength of 50 A·m^2 at 8 A applied current. Each coil is driven by an Advanced Motion Control 30A8 PWM servo drive, capable of 15 A continuous current, all powered by an Advanced Motion Control PS16L72 power supply with maximum DC output voltage of 72 V. Since each coil can be modeled as a RL circuit, the maximum frequency without attenuation, based on the amplifiers, power supply, coil resistance and inductance, is 97 Hz at 8 A.

2) Tri-axial Helmholtz Coils: The tri-axial Helmholtz Coils (Fig. 3b) are a system of three orthogonally nested sets of Helmholtz coils (note that each "Helmholtz coil" is actually two co-axial coils connected in series). Each Helmholtz coil generates a magnetic field that is optimally uniform at the center of the workspace, is aligned with the axis of the coil, and varies linearly with the electric current flowing through the coil. Three orthogonal coils enables the magnetic field vector to be assigned arbitrarily, with each Helmholtz coil corresponding to a basis direction in the field. Details of our system's construction is given in [21]. Each Helmholtz coil is driven by an Advanced Motion Controls S16A8 PWM analog servo drive, capable of 8 A continuous current with 24 V supplied by an Advanced Motion Control PS2X300W power supply. Since each Helmholtz coil can be modeled as a RL circuit, the maximum frequency without attenuation, based on the amplifiers, power supply, coil resistance and inductance, is 208 Hz at 8 A.

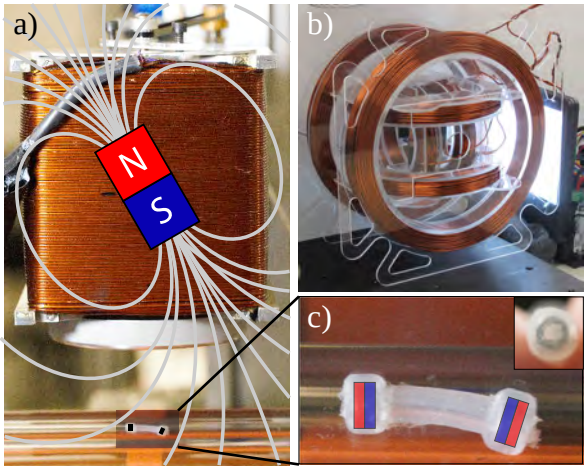

Fig. 3: (a) Experimental setup for rotating dipole fields using an Omnimagnet. (b) Experimental setup for rotating uniform fields using tri-axial Helmholtz coils. (c) Soft robot crawling through a tube. Inset shows the robot's internal lumen.

3) Soft Robot: Shown in Fig. 3c, the soft robots were fabricated using Dragon Skin 20 silicone, injected into a mold with two annular magnets threaded through a wire. The wire, once removed, creates a 1-mm-diameter lumen through the robot. The robot is 5 mm in diameter over the magnets, 2.5 mm in diameter at the central region, and 20 mm in total length. Two prototypes were made: one with alternating polarity and one with non-alternating polarity. The permanent magnets are Grade-N42 NdFeB magnets, axially magnetized, with 3 mm outer diameter, 1.5 mm inner diameter, 1.5 mm thickness, and with dipole strength of 0.0107 A·m^2.

B. Methods

All experiments involved placing the soft robot into a transparent tube with a 6 mm inner diameter and recording either the time it took for the robot to travel 20 mm or the distance traveled in 90 cycles, whichever occurred first. The value of 20 mm was chosen in order to stay within the small-angle approximation below the Omnimagnet, such that the distance from the center of the Omnimagnet to the soft robot was approximately constant. Trials were performed at frequency intervals between -18 Hz to 18 Hz (10 frequencies). Experiments were performed in sets of 20 random

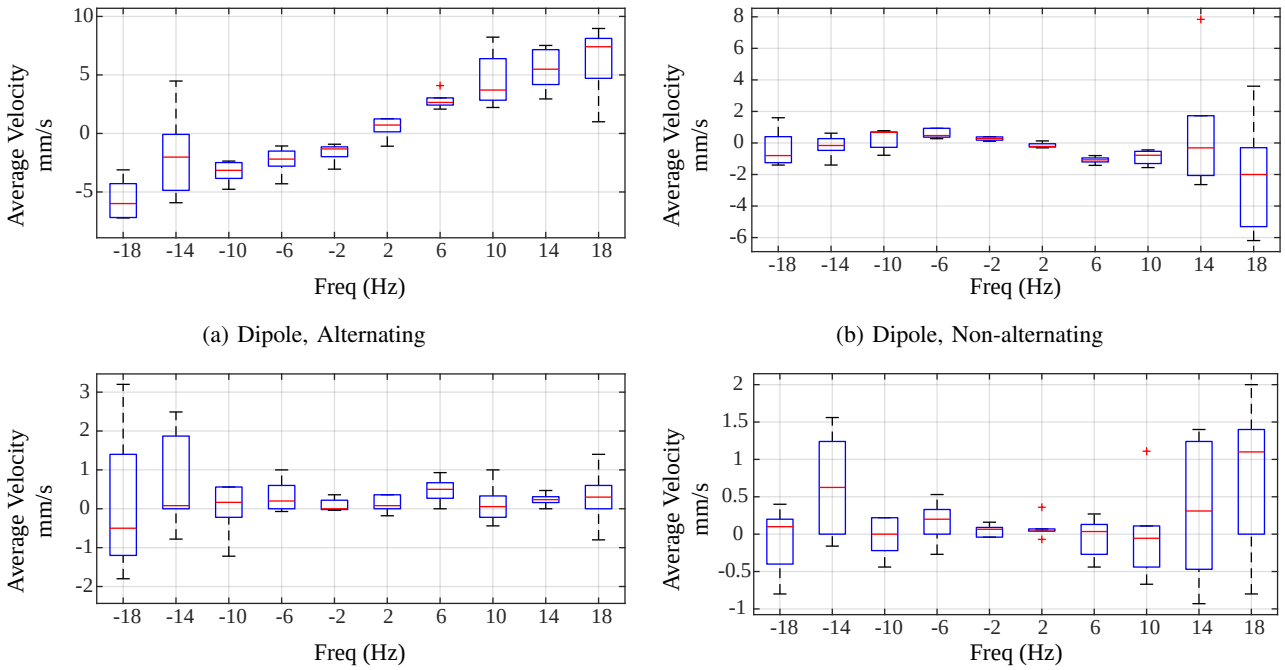

(a) Dipole, Alternating

(b) Dipole, Non-alternating

(c) Uniform, Alternating

(d) Uniform, Non-alternating

Fig. 4: Box-and-whisker plots of the average robot velocity for each of the scenarios considered in the experimental study.

combinations of frequency and magnet polarity. Six to eight sets of data were recorded for each frequency in Fig. 4.

For dipole (Omnimagnet) experiments, shown in Fig. 3a, the tube was placed in the horizontal plane below the Omnimagnet, 135 mm directly below its center (sufficiently far such that the point-dipole model is quite accurate). A dipole strength of 40 A·m^2 was rotated around an axis in the horizontal plane that is orthogonal to the axis of the tube and robot. This resulted in peak field strength of 1.72 mT at the robot, with the field strength varying by a magnitude of approximately two throughout the rotation cycle. Depending on the direction of travel (from pilot studies), the robot would be placed 10 mm either to the left or right of the tube's center. Rotating the dipole field would then cause the robot to travel directly under the Omnimagnet, where the field is the strongest, and after 20 mm of travel the robot would be 10 mm on the opposite side of the tube.

Uniform-field (tri-axial Helmholtz coils) experiments were performed at 1.72 mT field strength, which was the peak field value directly below the Omnimagnet in the rotating-dipole experiments described above. The tube was placed into the uniform workspace of the Helmholtz coils, with the robot placed directly at the center of the tube, since there was no expected direction of travel.

C. Results

The results of our experimental study are shown in Fig. 4. From these experiments we draw three main conclusions. (1) The alternating-polarity robot in a dipole field shows a strong correlation between the frequency of rotation and the robot velocity. The relationship appears approximately linear and consistent for low frequencies (-10 Hz to 10 Hz), but becomes more erratic at higher frequencies. (2) The non-alternating-polarity robot in a dipole field shows a small linear relationship between the frequency of field rotation and the robot velocity for low frequencies (-6 Hz to 6 Hz). The resulting velocity is slower and in the opposite direction of the alternating-polarity robot. At higher frequencies the average velocity is negligible, and the velocity in any given trial is erratic. (3) In uniform fields, regardless of the polarization of the magnets, there is no clear correlation between the field rotation frequency and the resulting robot velocity, with data straddling 0 mm/s at all frequencies.

IV. Numerical Verification

The movement of the robot is complex and involves magnetic forces, vibrations, surface inconsistencies, and contact between the tube and robot. However, the experimental results highlight two major factors that contribute to the robot propulsion: the nonuniformity of the rotating magnetic field, and the alternating polarity of the robot magnets. This section will attempt to explain why these two factors are important.

We have constructed a simple numerical simulation that gives a general idea of how the robot is deflecting and how it correlates with the experimental results. The structure is modeled as an elastic beam with roller constraints on the ends. These constrains allow the magnets to freely rotate and translate horizontally, but constrains them from translating vertically to approximate the constraint imposed by a lumen. The four cases that we consider are the same as those in the experiments, depicted in Fig. 2; they include the four

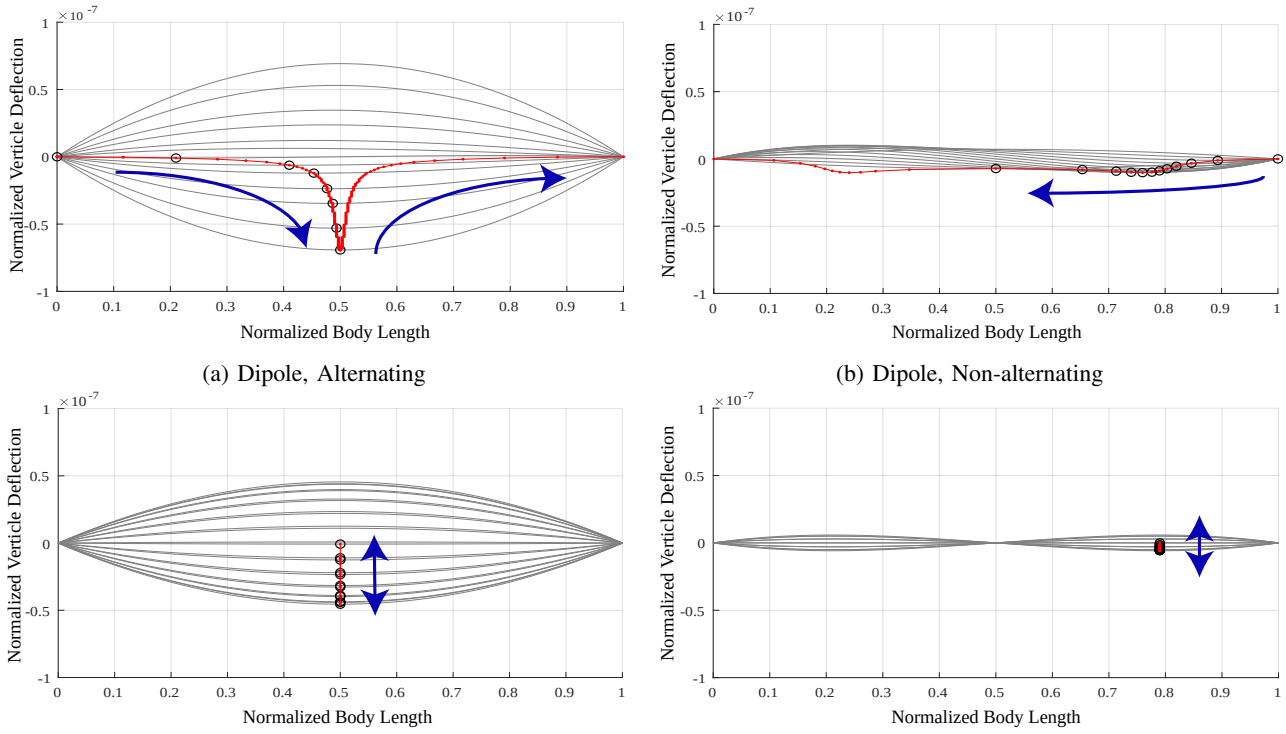

(a) Dipole, Alternating

(b) Dipole, Non-alternating

(c) Uniform, Alternating

(d) Uniform, Non-alternating

Fig. 5: Results of beam simulations for one rotation of the magnetic field, for each scenario in Fig. 2. Gray curves show the shape of the beam. Red curves with circle markers depict the lowest point on the beam for a half cycle. Blue arrows depict the motion of that point throughout the half cycle. The upper-left simulation represents our proposed concept.

combinations of field type (dipole or uniform) and magnet polarity (alternating or non-alternating).

For a given pair of magnetic torques applied at the ends of the beam, the deflection of the beam is calculated using the following differential equation

$$EI\frac{d^2}{dx^2}v(x) = M(x) \tag{4}$$

where x is a point along the beam, $v(x)$ is the vertical displacement at each point, $M(x)$ the bending moment at each point, E the modulus of elasticity, and I the second moment of area of the beam's cross-section. The local slope of the beam is calculated as $dv(x)/dx$. We assume small deflections. The solution for $v(x)$ is provided in the Appendix.

For a given magnetic field (dipole or uniform), we compute the torque on each of the embedded magnets using (1), and then solve for the beam deflection using (4). The slope at the beam's ends dictate the new orientation of the embedded magnets, and we use these new orientations to update the torque and re-solve for the beam's deflection. This process is repeated until the beam deflection converges on an equilibrium solution. After each update of the magnetic field by a small rotation, we use the previous beam solution to seed the search for the new beam solution.

In our simulations, we use a dipole field source located 135 mm above the beam, with a dipole strength of $\|\boldsymbol{m}_a\| = 40\,\text{A}{\cdot}\text{m}^2$. We used a beam with a length of 20 mm, and magnets with dipole strength of $\|\boldsymbol{m}\| = 0.0107\,\text{A}{\cdot}\text{m}^2$. These choices were used to stay consistent with the experimental setup (see Fig. 3c). We neglect the effects of magnetic forces.

Simulation results over one rotation of the magnetic field are shown by the grey lines in Fig. 5, with the circles and arrows highlighting the motion for half a cycle. The results suggest that the use of nonuniform magnetic fields is important: for both cases there is a clear traveling wave, whereas uniform fields will cause the beam to deflect in a standing wave. The results also suggest that alternating the polarities of the embedded magnets results in substantially larger deflections than with non-alternating polarity. This is because alternating the polarity results in excitation of the first bending mode of the beam, whereas non-alternating polarity excites the stiffer second bending mode.

This simple numerical study supports our fundamental conjecture and the main observations of the experimental study: the alternating-magnet robot travels faster that the non-alternating-magnet robot due to larger body deformations; deterministic directionality is created by a traveling wave induced by the dipole field, whereas the uniform field is expected to cause no net movement; and the non-alternating-magnet robot is expected to travel in the opposite direction from the alternating-magnet robot.

V. Conclusion

We described an actuation concept to enable a mesoscale soft robot to locomote through lumens. The concept com-

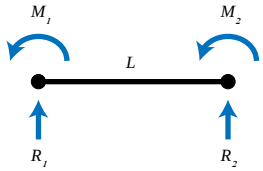

Fig. 6: Free body diagram of a beam with roller supports. The moments M_1 and M_2 represent the magnetic torques on the embedded magnets, which are assumed to be known.

prises a simple soft robot with two embedded permanent magnets with alternating magnetic polarity, and a rotating nonuniform (dipole) magnetic field that is swept over the robot, resulting in a traveling-wave undulatory motion that propels the robot forward and backward. We conducted experiments and numerical simulations to confirm the benefits of using nonuniform dipole fields over using uniform fields, as well as the benefits of alternating the polarity of the magnets embedded in the device.

Appendix

This appendix details the solution for the deflection $v(x)$ and slope $dv(x)/dx$ of an elastic beam, based on (4), used in Section III. We assume that the flexural rigidity of the beam (EI) is constant along the beam, and small deflections. The bending moment M acting on the beam at a distance x from the left end can be derived from the free body diagram in Fig. 6:

$$M(x) = -M_1 + R_1 x \tag{5}$$

Substituting (5) into (4) and integrating yields the slope of the beam, $dv(x)/dx$:

$$EI\frac{d}{dx}v(x) = -M_1 x + \frac{R_1}{2}x^2 + C_1 \tag{6}$$

Integrating again gives the deflection of the beam, $v(x)$:

$$EIv(x) = \frac{-M_1}{2}x^2 + \frac{R_1}{6}x^3 + C_1 x + C_2 \tag{7}$$

In total, there are four unknowns: R_1, R_2, C_1, and C_2. The boundary conditions provide two constraint equations:

$$v(0) = 0 \Rightarrow 0 = C_2 \tag{8}$$

$$v(L) = 0 \Rightarrow 0 = \frac{-M_1}{2}L^2 + \frac{R_1}{6}L^3 + C_1 L \tag{9}$$

Static equilibrium provides the other two constraints:

$$\sum F = 0 \Rightarrow R_1 + R_2 = 0 \tag{10}$$

$$\sum M = 0 \Rightarrow M_1 - R_1 L + M_2 = 0 \tag{11}$$

Solving (9)–(11) gives:

$$R_1 = \frac{M_1 + M_2}{L} \tag{12}$$

$$R_2 = \frac{-(M_1 + M_2)}{L} \tag{13}$$

$$C_1 = \frac{LM_1}{3} - \frac{LM_2}{6} \tag{14}$$

Acknowledgment

The authors would like to thank Sebastion Jenson and Dr. K. Lawrence DeVries for their technical contributions.

References

[1] A. J. Petruska and J. J. Abbott, "Optimal permanent-magnet geometries for dipole field approximation," *IEEE Trans. Magn.*, vol. 49, no. 2, pp. 811–819, 2013.

[2] S. E. Wright, A. W. Mahoney, K. M. Popek, and J. J. Abbott, "The spherical-actuator-magnet manipulator: A permanent-magnet robotic end-effector," *IEEE Trans. Robot.*, vol. 33, no. 5, pp. 1013–1024, 2017.

[3] A. J. Petruska and J. J. Abbott, "Omnimagnet: An omnidirectional electromagnet for controlled dipole-field generation," *IEEE Trans. Magn.*, vol. 50, no. 7, p. 8400810, 2014.

[4] A. W. Mahoney and J. J. Abbott, "Generating rotating magnetic fields with a single permanent magnet for propulsion of untethered magnetic devices in a lumen," *IEEE Trans. Robot.*, vol. 30, no. 2, pp. 411–420, 2014.

[5] S. H. Kim, S. Hashi, and K. Ishiyama, "Magnetic actuation based snake-like mechanism and locomotion driven by rotating magnetic field," *IEEE Trans. Magn.*, vol. 47, no. 10, pp. 3244–3247, 2011.

[6] J. Nam, G. H. Jang, S. M. Jeon, and G. H. Jang, "Development of a crawling microrobot with high steering capability and high stability to navigate through a sharply bent tubular environment," *IEEE Trans. Magn.*, vol. 50, no. 11, p. 8500704, 2014.

[7] E. Diller, J. Zhuang, G. Z. Lum, M. R. Edwards, and M. Sitti, "Continuous distributed magnetization profile for millimeter-scale elastomeric undulatory swimming," *Appl. Phys. Lett.*, vol. 104, p. 174101, 2014.

[8] W. Hu, G. Z. Lum, M. Mastrangeli, and M. Sitti, "Small-scale soft-bodied robot with multimodal locomotion," *Nature*, vol. 554, pp. 81–85, 2018.

[9] S. H. Kim, S. Hashi, and K. Ishiyama, "Hybrid magnetic mechanism for active locomotion based on inchworm motion," *Smart Mater. Struct.*, vol. 22, p. 027001, 2013.

[10] W. Wang, J. Lee, H. Rodrigue, S. Song, W. Chu, and S. Ahn, "Locomotion of inchworm-inspired robot made of smart soft composite (SSC)," *Bioinspir. Biomim.*, vol. 9, p. 046006, 2014.

[11] A. M. Bertetto and M. Ruggiu, "In-pipe inchworm pneumatic flexible robot," in *Proc. IEEE/ASME Int. Conf. Advanced Intelligent Mechatronics*, 2001, pp. 8–12.

[12] J. Lim, H. Park, J. An, Y. Hong, B. Kim, and B. Yi, "One pneumatic line based inchworm-like micro robot for half-inch pipe inspection," *Mechatronics*, vol. 18, pp. 315–322, 2008.

[13] D. Zarrouk, I. Sharf, and M. Shoham, "Conditions for worm-robot locomotion in a flexible environment: Theory and experiments," *IEEE Trans. Biomed. Eng.*, vol. 59, no. 4, pp. 1057–1067, 2012.

[14] A. S. Boxerbaum, K. M. Shaw, H. J. Chiel, and R. D. Quinn, "Continuous wave peristaltic motion in a robot," *Int. J. Robot. Res.*, vol. 31, no. 3, pp. 302–318, 2012.

[15] D. Chi and G. Yan, "From wired to wireless: A miniature robot for intestinal inspection," *J. Med. Eng. Technol.*, vol. 27, no. 2, pp. 71–76, 2003.

[16] B. J. Nelson, I. K. Kaliakatsos, and J. J. Abbott, "Microrobots for minimally invasive medicine," *Annu. Rev. Biomed. Eng.*, vol. 12, pp. 55–85, 2010.

[17] M. Sitti, H. Ceylan, W. Hu, J. Giltinan, M. Turan, S. Yim, and E. Diller, "Biomedical applications of untethered mobile milli/microrobots," *Proc. IEEE*, vol. 103, no. 2, pp. 205–224, 2015.

[18] P. Valdastri, M. Simi, and R. J. Webster III, "Advanced technologies for gastrointestinal endoscopy," *Annu. Rev. Biomed. Eng.*, vol. 14, pp. 397–429, 2012.

[19] L. J. Sliker and G. Ciuti, "Flexible and capsule endoscopy for screening, diagnosis and treatment," *Expert Rev. Med. Devices*, vol. 11, no. 6, pp. 649–666, 2014.

[20] A. J. Petruska, J. B. Brink, and J. J. Abbott, "First demonstration of a modular and reconfigurable magnetic-manipulation system," in *Proc. IEEE Int. Conf. Robotics and Automation*, 2015, pp. 149–155.

[21] A. W. Mahoney, J. C. Sarrazin, E. Bamberg, and J. J. Abbott, "Velocity control with gravity compensation for magnetic helical microswimmers," *Advanced Robotics*, vol. 25, pp. 1007–1028, 2011.